

AIR-Nets: An Attention-Based Framework for Locally Conditioned Implicit Representations

Simon Giebenhain

Bastian Goldlücke

University of Konstanz, Germany

{simon.giebenhain, bastian.goldluecke}@uni-konstanz.de

Abstract

This paper introduces Attentive Implicit Representation Networks (AIR-Nets), a simple, but highly effective architecture for 3D reconstruction from point clouds. Since representing 3D shapes in a local and modular fashion increases generalization and reconstruction quality, AIR-Nets encode an input point cloud into a set of local latent vectors anchored in 3D space, which locally describe the object’s geometry, as well as a global latent description, enforcing global consistency. Our model is the first grid-free, encoder-based approach that locally describes an implicit function. The vector attention mechanism from [62] serves as main point cloud processing module, and allows for permutation invariance and translation equivariance. When queried with a 3D coordinate, our decoder gathers information from the global and nearby local latent vectors in order to predict an occupancy value. Experiments on the ShapeNet dataset [7] show that AIR-Nets significantly outperform previous state-of-the-art encoder-based, implicit shape learning methods and especially dominate in the sparse setting. Furthermore, our model generalizes well to the FAUST dataset [1] in a zero-shot setting. Finally, since AIR-Nets use a sparse latent representation and follow a simple operating scheme, the model offers several exiting avenues for future work. Our code is available at <https://github.com/SimonGiebenhain/AIR-Nets>.

1. Introduction

Humans naturally possess a remarkable ability to perceive their environments in 3D. A few glimpses and head movements suffice to grasp the details of an object and understand its position within a scene. For machines such tasks remain difficult to solve.

For deep learning (DL) methods, choosing a suitable representation of 3D objects is defining large parts of the challenges to be solved, especially when generating 3D objects. For example, voxel grids provide great regularity and access to rich research results of convolutional neural networks (CNNs), but often have to be restricted in their resolution.

Other representations like point clouds and meshes live in a much sparser domain, but come with their own problems: while point clouds usually require an extreme number of points to describe detailed shapes, generating meshes with DL approaches is complicated, due to the discrete, combinatorial intricacies of generating face connectivities.

In order to avoid such problems, researches recently explored implicit neural representations [39, 34, 8], a fully continuous alternative for watertight objects, that is easily implemented and scales well on GPUs. The most common choices for the implicit function are signed distance functions (SDFs) and occupancy functions (zero outside and one inside of the object). In both cases a neural network approximates the implicit function of a watertight object, from which the 3D surface can be extracted by finding the zero level-set or decision boundary, respectively. While earlier work [34, 39, 8] always used a single latent vector to condition the implicit function on a specific object, recently research shifted to representing objects locally [9, 41, 27, 6, 53], resulting in greater representational power and higher generalization capabilities. Of these methods, [41, 9] are the only ones that use an encoder to infer the latent representation. The other models at least partially rely on running an optimization algorithm to infer an encoding, as inspired by [39].

In this paper, we propose *Attentive Implicit Representation Networks* (AIR-Nets), which are, to the best of our knowledge, the first encoder-based local implicit shape learning model that purely operates in the point cloud domain. AIR-Nets utilize the vector attention mechanism proposed in [62] to encode input points into a sparse set of locally anchored latent vectors and a single global latent vector. By representing the geometric structure of objects as a composition of local descriptors, AIR-Nets exhibit highly detailed reconstructions and great generalization capabilities. The occupancy function is modeled by our proposed attentive decoder, which aggregates information from the global and nearby local latent vectors. These extracted features are finally transformed into occupancy predictions by a simple feed-forward network (FFN). The resulting archi-

ture is permutation invariant and translation equivariant, see figure 1 for a schematic illustration. Therefore, compared to the grid-based methods of [9, 41], which represent shapes with features drawn from the dense voxel grid of a 3D CNN, AIR-Nets avoid any discretization, while representing objects in a more compressed fashion. This allows for easy adoptions in downstream tasks, new domains or translation to a probabilistic generative setting.

In summary, our contributions are the following:

- We propose the AIR-Net framework, a highly effective, purely point cloud based architecture for local, implicit shape representations, that modularly encodes objects into a set of locally anchored latent vectors.
- We propose a novel attention-based set abstraction method that outperforms the common maxpooling based downsampling.
- Furthermore, we propose an attentive decoder in conjunction with our latent shape representation and show the importance of an expressive decoder compared to a simple interpolation based decoder.
- AIR-Nets significantly outperform state-of-the-art implicit representations methods in 3D reconstruction from point clouds and generalize well from the ShapeNet to the FAUST dataset in a zero-shot setting.

2. Related Work

Designing DL methods for geometric objects heavily depends on the chosen representation for 3D shapes. We therefore present a brief overview of DL architectures for geometric data processing in section 2.1, while models for shape generation and 3D reconstruction are discussed in section 2.2.

2.1. Geometric Data Processing

This section provides a brief overview of methods for discriminative tasks on geometric data. For a great theoretical approach to geometric DL and a more detailed overview of this rapidly growing field we recommend [3].

Voxel Processing. Representing 3D objects as voxel grids and generalizing tools from 2D CNNs is possibly the most straight forward way to process 3D shapes, *e.g.* [2, 50]. Despite their cubic memory demands, 3D CNNs are frequently adopted, *e.g.* in the closely related works [34, 41, 9] or in 3D object detection [47], which uses sparse convolutions [19] to lessen the memory footprint.

Point Cloud Processing. Designing DL models for point clouds is complicated, since they have to be permutation invariant and point clouds often exhibit very irregular structure and densities. Early approaches process points individually before applying permutation invariant pooling operations [42, 43]. More recent approaches utilize

graph convolutional networks (GCN), originally introduced in [4, 12, 29, 17]. For example [57, 61, 59] use GCNs by locally connecting points in the point cloud.

Others define continuous convolution operations around points, *e.g.* [56, 58, 52]. More models are surveyed in [22].

Inspired by the recent success of Transformers [54], their natural permutation invariance and ability to work with a wide variety of data structures, *e.g.* sequences [54, 45], images [13] or abstract objects [5], recent work builds upon attention mechanisms to process point clouds [62, 21, 14]. Our approach leverages the ideas from [62], which uses the generalized vector attention mechanism from [60], instead of the classical scalar-valued dot-product attention from [54]. Note that attention mechanisms can be thought of a special kind of graph convolution operation, as pointed out in [3], *i.e.* full attention operates on the fully connected graph, while the local attention of [62] operates on the k nearest neighbor (k NN) graph. Finally, we want to highlight some approaches to obtain SE(3)-equivariant processing modules [15, 24, 46].

Mesh Processing. Methods for meshes are closely related to GCNs, which are, however, insensitive to the local geometry of the mesh. Therefore, several different approaches to obtain geometry aware convolutions exist [33, 36, 23]. We refer to [3] for a detailed overview.

2.2. Shape Generation and Reconstruction

Contrary to the previous section, this section is solely concerned with models that produce a 3D shape as output, *e.g.* generative or 3D reconstruction models. As point clouds do not unambiguously describe a surface, models generating point clouds are not discussed here.

Voxel Grids. Generating high resolution voxel grids is less suitable, due to a high memory footprint. While it is possible to design more efficient octree-based 3D CNN architectures [50, 25], these methods are still limited by a resolution of 256^3 and are complicated to implement.

Meshes. Usually mesh generation is limited to a single topology of a *template* mesh. Therefore the generation task condenses to predicting the location of all vertices. Such models [18, 44] achieve impressive results in this less general scenario. Template-free mesh generation is less common, since predicting a variable number of vertices and their adjacencies is quite complicated. [37] build on Transformers [54], by viewing the problem as a sequence generation problem and auto-regressively predicting all vertices and then all n -gon faces. A similar approach for general graphs is proposed in [30].

Implicit Continuous Functions. To avoid some of the above mention complications, continuous implicit functions like the (truncated) SDF and occupancy function have become a rapidly growing field of research for 3D representations of *watertight* objects. Due to their continuity, implicit

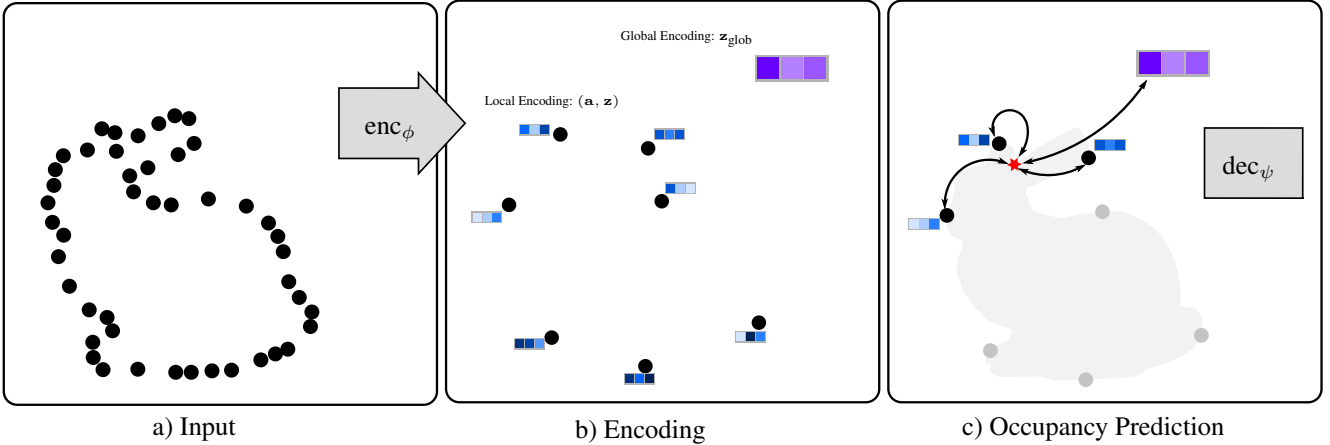


Figure 1. **Model Overview:** This figure illustrates the operating scheme of AIR-Nets simplified to 2D. The input point cloud (left) is encoded into a global latent vector (purple) and a much sparser point cloud, where a local latent vector (blue) is attached to each point (middle). When queried with a spatial coordinate (red star), the decoder network locally extracts latent information using an attention mechanism, where the global descriptor acts as query and the local ones act as keys and values, to predict an occupancy value (right).

functions are well-suited for DL and can be easily implemented as a simple FFN. Such models mainly differ in two aspects. First, some models use an encoder network to determine the latent representation [34, 8], while others are *encoder-less* [39, 48, 20], which eliminates the need to design an encoder for geometric observations such as point clouds. Instead they directly optimize for the latent representation of each object, causing long inference time for previously unseen objects.

The second major difference lies in the conditioning of the implicit function on a specific object. While early approaches use a single latent vector to represent a shape [34, 8, 39], recent models use multiple local latent descriptors, resulting in high-quality reconstructions and better generalization. The encoder-based approaches [9, 41] represent the implicit function locally using features drawn from the voxel grid of a CNN. Compared to these grid-based approaches, our model purely operates in the point cloud domain, avoiding discretization losses and quadratic/cubic scaling with the resolution, and resulting in a much sparser and more compressed encoding.

Several approaches to encoder-less local representations exist [53, 27, 6]. These methods, however, cannot effectively reconstruct large regions devoid of any observations.

The models in [16] and [53] are similar to ours, since they also use a sparse set of spatially anchored latent vectors, but construct their implicit function differently, by interpolating between multiple implicit functions using 3D Gaussians. Our model uses a computationally more expressive and slightly less interpretable procedure to parameterize the implicit function.

Using a slightly different approach, [10] models an unsigned distance field, relaxing the assumption of watertight

objects, but rendering the extraction of the zero level set impossible. Instead very dense surface point clouds and rendered images of the surface can be generated.

3. Attentive Implicit Representation Networks

AIR-Nets offer an encoder-based implicit shape learning framework, which finds a compromise between conditioning the implicit function on a single latent vector [34, 8] and a dense voxel grid of features [9, 41]. It does so by encoding an input point cloud into a sparse set of M locally anchored latent vectors and a global latent vector. Therefore AIR-Nets are encouraged to understand objects as a composition of local shapes, leading to better generalization capabilities and a higher capacity to reconstructed rich details. Figure 1 illustrates the operating scheme of AIR-Nets.

From a high-level point of view, the encoder

$$\text{enc}_\phi : \mathbb{R}^{N \times (3+d_0)} \rightarrow \mathbb{R}^{M \times (3+d)} \times \mathbb{R}^d, \quad (1)$$

maps the input point cloud $P \in \mathbb{R}^{N \times 3}$ and features $F \in \mathbb{R}^{N \times d_0}$ to anchors \mathbf{a} , local latent vectors \mathbf{z} and the global latent vector \mathbf{z}_{glob} . The complete encoder architecture is described in section 3.2, after reviewing the vector attention mechanism of [62] in section 3.1.

The implicit function is modeled by the decoder

$$\text{dec}_\psi : \mathbb{R}^{M \times (3+d)} \times \mathbb{R}^d \times \mathbb{R}^3 \rightarrow [0, 1], \quad (2)$$

which takes queried coordinates $(x, y, z) \in \mathbb{R}^3$ alongside the encoding as input, and predicts the probability for (x, y, z) to be inside of the observed watertight object. The decoder aggregates information from nearby local latent vectors using vector cross attention. Finally, a simple FFN maps the locally aggregated information to an occupancy

prediction. More details about the decoder are presented in section 3.3.

3.1. Background: Point Transformer [62]

The vector attention mechanism of [62] serves as core processing module throughout the complete AIR-Net architecture. Therefore, this section formulates their vector attention mechanism in the more general form of a cross attention operator. The vector cross attention (VCA) operator

$$\text{VCA}: \mathbb{R}^{N_q \times (3+d_q)} \times \mathbb{R}^{N_{kv} \times (3+d_{kv})} \rightarrow \mathbb{R}^{N_q \times d} \quad (3)$$

maps a *query* point cloud $P_q \in \mathbb{R}^{N_q \times 3}$ and features $X_q \in \mathbb{R}^{N_q \times d_q}$ and a *key-value* point cloud $P_{kv} \in \mathbb{R}^{N_{kv} \times 3}$ and features $X_{kv} \in \mathbb{R}^{N_{kv} \times d_{kv}}$ to output features $X' \in \mathbb{R}^{N_q \times d}$. From a high level perspective, attention mechanisms can be thought of as a differentiable information routing schemes, where queries describe the sought for information among the key-value tokens.

Internally, queries $Q = (P_q, F_q) = (P_q, X_q W_q)$ and keys $K = (P_{kv}, F_k) = (P_{kv}, X_{kv} W_k)$ are derived using linear transformations $W_q \in \mathbb{R}^{d_q \times d}$ and $W_k \in \mathbb{R}^{d_{kv} \times d}$ on the features. Information around the i -th query is then aggregated from its neighborhood \mathcal{N}_i (i.e. k NN) using

$$X'_i = \sum_{j \in \mathcal{N}_i} n(s(Q_i, K_j)) \odot V_{ij}, \quad (4)$$

where n denotes the channel-wise softmax function, \odot the Hadamard product of two vectors and

$$V_{ij} = F_{kv_j} W_v + \delta(P_{q_i} - P_{kv_j}) \quad (5)$$

the values. Note that defining the values as such, extends the standard formulation of the attention mechanism from [55] due to the dependence on i . Including positional information modelled by a two-layer multilayer perceptron (MLP) with a single ReLU activation $\delta: \mathbb{R}^3 \rightarrow \mathbb{R}^d$ was empirically found to be beneficial [62]. The original motivation for δ lies, however, in the similarity function

$$s(Q_i, K_j) = \gamma(F_{q_i} - F_{k_j} + \delta(P_{q_i} - P_{kv_j})), \quad (6)$$

which calculates vector valued similarities between queries and keys using δ and another two-layer MLP γ . Using this more general VCA operator, vector self attention (VSA), as used in the Point Transformer, can be finally defined as

$$\text{VSA}(X) := \text{VCA}(X, X). \quad (7)$$

We refer to the supplementary for a formulation of VCA and VSA in the language of graph neural networks.

3.2. Encoder

This section describes the encoder architecture, as illustrated in figure 3. The two main modules of the encoder

are the *point transformer block* (PTB) and *attentive set abstraction module* (SetAbs), which we describe later. Both are based on the VSA and VCA modules, as defined above. The point transformer block

$$\text{PTB}(X) := \text{BN}(X + \text{VSA}(X)) \quad (8)$$

simply encapsulates VSA, a residual connection and a BatchNorm (BN) layer [26]. Note that the point’s positions remain unaltered. We form local neighborhoods using k NN with $k_{\text{enc}} = 16$, to impose an effective inductive bias and limit memory consumption.

Translation Equivariance. Here, we want to stress that the whole network is translation equivariant, since both VSA and VCA modules only use relative positions. Therefore the computation of features is invariant, which are, however, spatially anchored and hence become equivariant. In order to preserve this equivariance it is important to not include the input coordinates as features in the initial encoding PTB. If the input point cloud does not carry any other features besides the spatial coordinates (i.e. F is empty), eq. (5) and (6) have to be modified such that only the δ -terms remain.

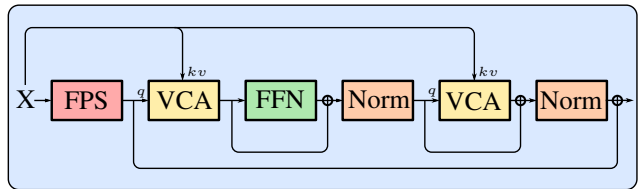


Figure 2. The proposed set abstraction module SetAbs_n first selects n central points using FPS. The central points act as queries in a VCA module that aggregates information from their neighborhoods of size $k_{\text{enc}} = 16$. A second round of attention lessens the dependence on the initial, random selection of the central point. Here FFN composes a 2-layer MLP, skip connection and BN layer.

Downsampling. In many learning tasks, downsampling is a crucial component to encourage abstract and robust reasoning and reduce the computational requirements. AIR-Nets follow the typical downsampling scheme applied in most point cloud processing networks [43, 62, 21]. The prevalent procedure is to subselect points using farthest point sampling (FPS) as a simple heuristic and then build local neighborhoods around the selected points (from now on called *central* points) using a grouping mechanism, like ball queries [43] or k NN. Finally, each neighborhood is abstracted into the new representative features for the central point’s position using a permutation invariant function. Transforming point features independently with a small, shared MLP followed by maxpooling is the most common choice for the set abstraction step. We argue, however, that maxpooling is sub-optimal, since each point is treated

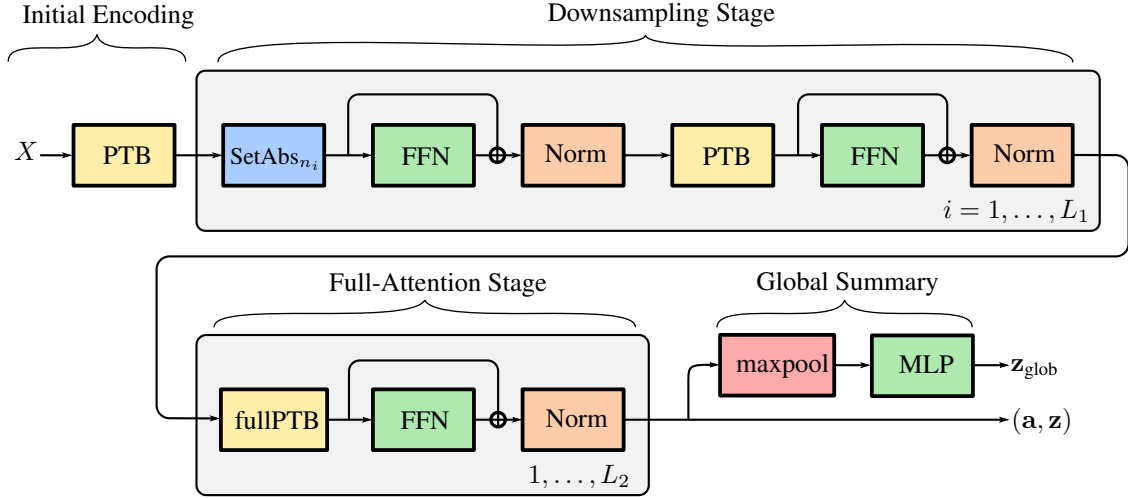


Figure 3. **Encoder architecture:** After an initial encoding, the point cloud is repeatedly downsampled using L_1 SetAbs modules. To preserve more information, an additional PTB is added before the next downsampling step. Each downsampling layer also includes a FFN, skip connection and normalization layer after each block involving attention, as proposed in [54]. In the same style, L_2 full-attention PTBs are used to promote global information exchange, producing local descriptors \mathbf{z} and anchors \mathbf{a} . The global latent vector \mathbf{z}_{glob} is derived using maxpooling. All normalization layers are realized as BatchNorm layers [26].

equally, which becomes especially problematic in very diverse neighborhoods and in the presence of outliers. As an alternative to maxpooling, we propose to use two iterations of vector cross attention. The complete attentive set abstraction module is depicted in figure 2 and adheres to the function signature

$$\text{SetAbs}_{n'} : \mathbb{R}^{n \times (3+d)} \rightarrow \mathbb{R}^{n' \times (3+d)}, \quad (9)$$

where n' specifies the desired output cardinality. The intuition behind the module is that the central point attends to its k_{enc} neighbors (including itself) and builds a summary thereof. However, since this summary strongly depends on the (random) selection of the central point, a second round of attention refines the summary to lessen this bias.

Using SetAbs as a downsampling module, the point cloud is repeatedly downsampled using L_1 downsampling layers with intermediate cardinalities n_1, \dots, n_{L_1-1} , until a cardinality of $n_{L_1} := M$ is reached. In order to give the model an opportunity to compute more meaningful features before the next SetAbs, each downsampling layer also includes a regular PTB.

Full Attention. After the input is reduced to the desired cardinality M , L_2 full attention layers facilitate global information exchange (instead of k NN, all points are considered as neighbors). Gaining a global understanding of the object is important in order to exploit symmetries and supplement information to regions with little observations. The resulting point cloud and features serve as anchors \mathbf{a} and local latent vectors \mathbf{z} respectively.

Finally, the global summary \mathbf{z}_{glob} is obtained using global maxpooling followed by a 2-layer MLP.

3.3. Decoder

Provided with an encoding $(\mathbf{a}, \mathbf{z}), \mathbf{z}_{\text{glob}}$ of a watertight object, the decoder

$$\text{dec}_{(\mathbf{a}, \mathbf{z}), \mathbf{z}_{\text{glob}}} : \mathbb{R}^3 \rightarrow [0, 1], (x, y, z) \mapsto o \quad (10)$$

models the occupancy function, which maps coordinates (x, y, z) to the probability o to be inside of the object.

Due to the compressed nature of the encoding, the relevant information for an occupancy prediction is not as regularly structured and not as readily available as in grid-based approaches [41, 9]. Consequently, we find that using an expressive enough decoder, capable of effectively extracting the relevant information in many different scenarios, is crucial, as ablated in section 4.6. Therefore we propose to use vector cross attention to extract the relevant information

$$\mathbf{z}_{\text{loc}} = \text{VCA}(X_q, X_{kv}), \quad (11)$$

where $X_q = ((x, y, z), \mathbf{z}_{\text{glob}})$ is the single element query and $X_{kv} = (\mathbf{a}, \mathbf{z})$ constitutes key-value tokens. To further encourage a local encoding and reduce the runtime and memory complexity, the attention is limited to the k_{dec} nearest local latent vectors. Using \mathbf{z}_{glob} as query provides context information, adapting the local information aggregation appropriately to the given scenario. Furthermore, we find that additionally including \mathbf{z}_{glob} in the key-values achieves slightly better results. For this token alone we remove the delta term from eq. (5), as it is free of any spatial location.

The final occupancy probability o is predicted using the same FFN as in [38, 41].

3.4. Training and Inference

The model parameters ϕ and ψ are trained using a dataset of T watertight shapes S_i , with inputs $X_i = (P_i, F_i)$ and ground truth $Y_i = (Q_i, O_i)$, where Q_i denotes the 3D coordinates and O_i the corresponding ground truth occupancy values. Note that in all of our experiments P_i is the only observation (*i.e.* F_i does not carry any additional features). We optimize the parameters ϕ and ψ using the loss

$$\mathcal{L} = \sum_{i \in I} \sum_{j \in J} L(\text{dec}(\text{enc}(X_i), Q_{i,j}), O_{i,j}), \quad (12)$$

where I is the mini-batch index, J subselects 1.000 ground truth points and $L(\hat{o}, o) = -[o \cdot \log(\hat{o}) + (1 - o) \cdot \log(1 - \hat{o})]$ is the binary cross-entropy loss.

During inference time, meshes are reconstructed using the MISE [34] algorithm, which is an efficient way of extracting the isosurface using the marching cubes algorithm [32].

4. Experiments

We conduct extensive experiments to demonstrate the representational power and generalization capability of AIR-Nets in 3D shape learning. In section 4.4 we evaluate our model on 3D shape reconstruction from point clouds using the ShapeNet [7] dataset and compare against a set of representative baseline models. Furthermore, we evaluate the zero-shot generalization capabilities of all these models by applying them to the FAUST [1] dataset in section 4.5. Finally, we conduct controlled ablation studies in section 4.6 to validate several design choices of AIR-Nets.

4.1. Datasets

We use all 13 object classes of the well-known ShapeNet dataset and use the common training split of [11]. Furthermore, we use two differently pre-processed versions of the dataset, \mathcal{D}_A [9] and \mathcal{D}_B [34] and refer to the respective papers for more details. Note that therefore, the results cannot be directly compared across datasets. The main difference of these datasets is, however, the spatial distribution of the supervision points Q_i . Dataset \mathcal{D}_A samples Q_i close to the boundary of the ground truth surface, in order to supervise more in the most crucial region. Contrary \mathcal{D}_B samples Q_i uniformly in the unit cube. Furthermore, we follow [9] and use \mathcal{D}_A without measurement noise and follow [34, 41] to use \mathcal{D}_B with additive Gaussian measurement noise with a standard deviation of 0.005.

Additionally we evaluate all models on the test set of the FAUST dataset without pre-processing the meshes.

4.2. Baselines and Evaluation Metrics

We compare against all state-of-the-art encoder-based implicit shape representation models. We compare against *Occupancy Networks* (ONets) [34], as representative of

models using a single global latent representation. We additionally compare against *Implicit Feature Networks* (IF-Nets) [9] and *Convolutional Occupancy Networks* (ConvONets) [41], as representatives for encoder-based local implicit representations. The former uses a 3D CNN to encode the input and for the latter we chose its best performing variant, which projects the 3D input points on the xy , xz and yz -plane, and uses 2D CNNs.

The quality of the reconstructions is evaluated using the four most established metrics: the *volumetric intersection over union* (IoU), the L_1 -*Chamfer-Distance* (L_1 -CD), the *normal consistency* (NC) [34] and the *F-score* [51].

4.3. Implementation Details

We implemented our models using PyTorch [40] and trained all models using the Adam optimizer [28] and a batch size of 64. For AIR-Nets the initial learning rate is set to $5e^{-4}$ and decayed with a factor of 0.2 after every 200 epochs. For all baselines we used the official code release and training procedure. All models were trained until the validation loss ceased to improve. We select the epoch with the best validation loss for evaluation.

Unless stated otherwise the internal dimensions in all linear layers, the VCA and VSA modules is 256. The number of anchors is $M = 100$ and the number of downsampling layers is $L_1 = 2$ for all experiments. When the number of input points $N = 300$, we set the intermediate cardinality of the downsampling stage to $n_1 = 200$. When $N = 3000$, we use $n_1 = 500$ instead. The number of full attention layers is $L_2 = 3$. The neighborhood sizes are $k_{\text{enc}} = 16$ and $k_{\text{dec}} = 7$ unless stated otherwise. The VCA module in the decoder uses 200 dimensions to reduce memory demands. For the final FFN we use 5 layers and a hidden dimensionality of 128. Some of these hyperparameters as well as a runtime and memory analysis are provided in the supplementary.

4.4. 3D Reconstruction from Point Clouds

In this section, AIR-Nets and the various baseline models are separately trained and evaluated on the 3D reconstruction task from point clouds on \mathcal{D}_A and \mathcal{D}_B . Following [9], we additionally distinguish between a sparse and dense setting. In the sparse setting, inputs are composed of 300 points sampled uniformly on the ground truth object surface, while 3000 points are used for the dense setting.

While the sparse setting assesses the model’s capabilities to complete geometric structures, the dense setting tests the representational capacity and ability to preserve fine details.

4.4.1 Noise-free Observations from \mathcal{D}_A

For this experiment all models are trained and evaluated on \mathcal{D}_A , which is noise-free. The results presented in table 1 clearly show that AIR-Nets outperform all baselines by a

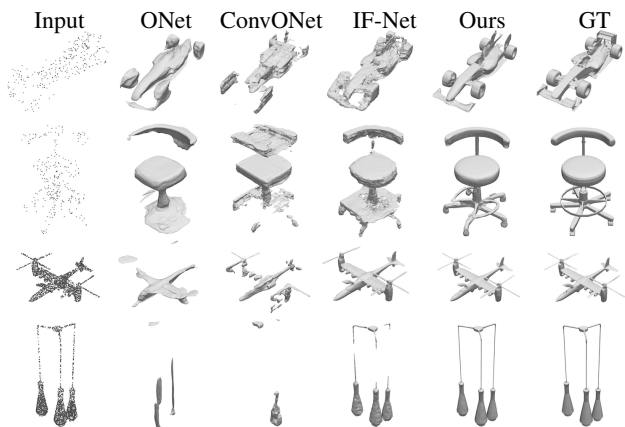


Figure 4. **3D Reconstructions on \mathcal{D}_A** : Qualitative comparison on less common objects. The top two rows show the sparse setting, while the bottom two show results in the dense setting. Best viewed digitally and zoomed-in.

| | Model | IoU \uparrow | L_1 -CD \downarrow | NC \uparrow | F-Score \uparrow |
|--------------|----------|----------------|------------------------|---------------|--------------------|
| Sparse Input | ONet | 0.724 | 0.0094 | 0.878 | 0.808 |
| | ConvONet | 0.723 | 0.0084 | 0.876 | 0.841 |
| | IF-Net | 0.772 | 0.0060 | 0.885 | 0.885 |
| | Ours | 0.913 | 0.0032 | 0.95 | 0.964 |
| Dense Input | ONet | 0.704 | 0.0100 | 0.874 | 0.786 |
| | ConvONet | 0.752 | 0.0074 | 0.894 | 0.881 |
| | IF-Net | 0.883 | 0.0034 | 0.948 | 0.983 |
| | Ours | 0.958 | 0.0024 | 0.972 | 0.991 |

Table 1. **Quantitative Results on \mathcal{D}_A**

large margin. Especially in the sparse setting AIR-Nets are dominant. They even outperform all baselines from the dense setting. We believe that full self-attention in AIR-Nets especially helps in the sparse setting to exploit global symmetries and long-range dependencies, which is less relevant in the dense setting due to high-quality observations. Note that in the noise-free scenario, the discretization procedures in ConvONets and IF-Nets have a more relevant negative effect. Also, note that ConvONets overfitted in both settings before reaching their full potential. The qualitative results presented in figure 4 confirm the great effectiveness of AIR-Nets. On sparse input data AIR-Nets are capable to reconstruct a surprising amount of detail, while maintaining smooth surfaces. While IF-Nets also produce pleasing results in the dense setting, their reconstruction suffers from bumpy artefacts and often misses fine details. More qualitative results are provided in the supplementary.

4.4.2 Noisy Observations from \mathcal{D}_B

In this section, all models are trained and evaluated on \mathcal{D}_B , to test the model’s performance in the presence of noise. Table 2 confirms the dominance of AIR-Nets in the sparse setting. In the dense setting, IF-Nets are performing simi-

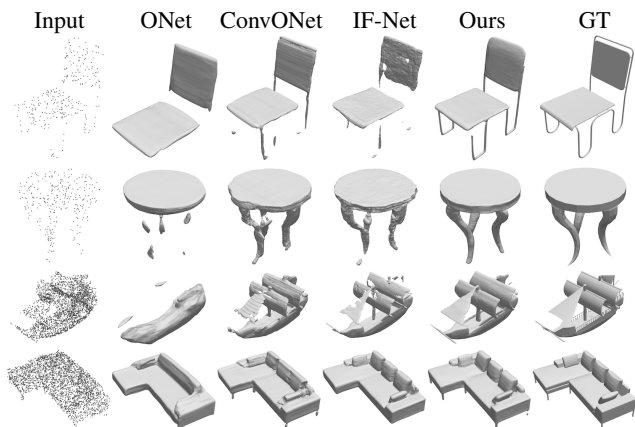


Figure 5. **Qualitative Results on \mathcal{D}_B** : Same structure as figure 4.

| | Model | IoU \uparrow | L_1 -CD \downarrow | NC \uparrow | F-Score \uparrow |
|--------------|----------|----------------|------------------------|---------------|--------------------|
| Sparse Input | ONet | 0.755 | 0.0084 | 0.891 | 0.797 |
| | ConvONet | 0.801 | 0.0061 | 0.908 | 0.871 |
| | IF-Net | 0.763 | 0.0070 | 0.895 | 0.84 |
| | Ours | 0.869 | 0.0047 | 0.929 | 0.93 |
| Dense Input | ONet | 0.758 | 0.0082 | 0.893 | 0.802 |
| | ConvONet | 0.888 | 0.0040 | 0.935 | 0.953 |
| | IF-Net | 0.924 | 0.0030 | 0.951 | 0.985 |
| | Ours | 0.925 | 0.0033 | 0.952 | 0.978 |

Table 2. **Quantitative Results on \mathcal{D}_B**

larly well. Partly, this can be explained due to the fact that IF-Nets are less effected by the noise, since they discretize the input. The qualitative results in figure 4 show that AIR-Nets are still capable of producing smooth surfaces, despite the presence of noise. IF-Nets again have a slight tendency to lose thin details, while AIR-Nets tend to reconstruct thin structures too thick (*e.g.* see feet of sofa and the sail).

Another very interesting finding is that all baselines seem to be performing better on \mathcal{D}_B , despite the presence of noise. We believe that the uniformly distributed supervision points of \mathcal{D}_B could be better suited for all baseline models or that they overfit slower due to the presence of noise.

4.5. Zero-Shot Generalization

In order to evaluate the generalization ability of the models, we evaluate their 3D reconstruction quality on the FAUST [1] dataset in a zero-shot fashion. We chose the best performing model for each model-type trained in the dense setting, *i.e.* for all baselines the dense models trained on \mathcal{D}_B . For the sake of completeness, we evaluate both dense AIR-Net models. The input point clouds are generated by uniformly sampling 3000 points on the surface of the ground truth mesh, which already contains real measurement noise, as well as occasional holes, violating the watertightness of the objects (*e.g.* see feet of ground truth in figure 6). Hence the IoU is calculated using the implicit

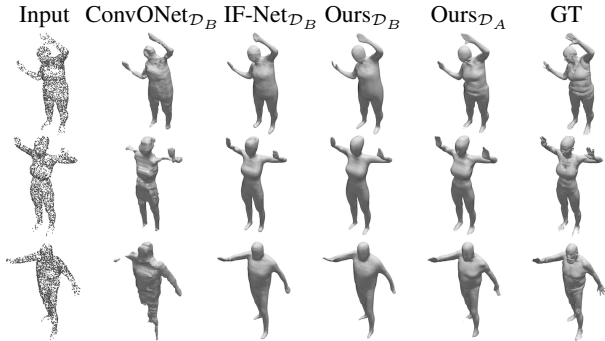


Figure 6. **Zero-Shot 3D Reconstructions on FAUST.** Subscripts denote which dataset the models were trained on.

waterproofing algorithm from [9]. Quantitative and qualitative results are presented in table 3 and figure 6, respectively. The results show that IF-Nets and AIR-Nets generalize best, which we account for by their translation equivariance. AIR-Nets trained on \mathcal{D}_A , however, reconstruct significantly more details.

| Model | IoU \uparrow | L_1 -CD \downarrow | NC \uparrow | F-Score \uparrow |
|-----------------------------|----------------|------------------------|---------------|--------------------|
| ONet $_{\mathcal{D}_B}$ | 0.149 | 0.05416 | 0.591 | 0.149 |
| ConvONet $_{\mathcal{D}_B}$ | 0.634 | 0.01066 | 0.816 | 0.661 |
| IF-Net $_{\mathcal{D}_B}$ | 0.888 | 0.00354 | 0.942 | 0.958 |
| ours $_{\mathcal{D}_B}$ | 0.891 | 0.00353 | 0.942 | 0.957 |
| ours $_{\mathcal{D}_A}$ | 0.920 | 0.00290 | 0.951 | 0.964 |

Table 3. **Quantitative Results of the Zero-Shot Reconstructions on the FAUST dataset.**

4.6. Ablation Studies

This section presents experiments to validate the design of the *downsampling stage* and *full-attention stage* (see figure 3), as well as, the proposed decoder. For this purpose we construct the most simple baseline composed of a PointNet++ [43] inspired encoder, no full-attention and interpolation based decoder, as used as a baseline in [41]. We consecutively improve the model by replacing the interpolation-based decoder, with the proposed attention-based decoder, by adding full-attention layers and by using the proposed downsampling stage. The results for these four models are presented in table 4, indicating the benefits of each individual module. Additionally, we included a model using the common maxpooling-based set abstraction instead of the proposed attentive set abstraction module, showing that the proposed set abstraction method compares favourably.

Finally, we compare the proposed decoder against two alternatives in the bottom two rows of table 4, showing the great importance of using an expressive decoder. More details and experiments are provided in the supplementary.

| Model | IoU \uparrow | L_1 -CD \downarrow | NC \uparrow | F-Score \uparrow |
|-------------------|----------------|------------------------|---------------|--------------------|
| PN::interp | 0.444 | 0.03959 | 0.763 | 0.336 |
| PN::ours | 0.807 | 0.00528 | 0.891 | 0.890 |
| PN:3full:ours | 0.859 | 0.00430 | 0.926 | 0.930 |
| PT:3full:ours | 0.888 | 0.00374 | 0.940 | 0.952 |
| ours:3full:ours | 0.896 | 0.00356 | 0.945 | 0.957 |
| ours:3full:interp | 0.801 | 0.00770 | 0.904 | 0.874 |
| ours:3full:LDIF | 0.839 | 0.00501 | 0.917 | 0.912 |

Table 4. **Component Ablation:** Models are named as composition of 3 sections, the encoder, potential full attention and the decoder. PN and PT stand for PointNet++ and Point Transformer respectively. An empty middle section denotes the lack of full self-attention layers, *interp* denotes a decoder interpolating between features [41] and *LDIF* denotes a decoder interpolating between implicit functions [16]. Note, that the 3rd to last row is the complete AIR-Net. All models were trained on \mathcal{D}_A in the sparse setting for 300 epochs and evaluated on 2000 test examples.

5. Discussion and Conclusion

In this work, we have introduced AIR-Nets, a novel encoder-based local implicit shape learning model operating purely on point clouds. Building on the local attention mechanism from [62], we propose a fully translation equivariant framework for 3D shape reconstruction. AIR-Nets represent shapes by a global latent vector and a set of local latent vectors anchored in 3D space. This local, modular representation allows for highly detailed reconstruction and promotes generality. Our experiments show that AIR-Nets outperform previous state-of-the-art methods in 3D reconstruction on the ShapeNet dataset by a large margin. Furthermore, AIR-Nets generalize well to the FAUST dataset in a zero-shot setting. Ablation studies validate several of our encoder components and show the benefits of the proposed, attention-based decoder.

Finally, the AIR-Net framework offers several exciting avenues for future work. First, since our framework is relatively new compared to 3D CNNs, we believe that it offers great potential for future extensions, as well as, applications to large-scale scenes [41] and joint implicit appearance modelling, *e.g.* [35, 49, 31]. Second, compared to IF-Nets and ConvONets, the relative sparsity of the latent representation renders AIR-Nets more suitable for a probabilistic, generative setting, which could be useful for single-view 3D reconstruction. Finally, our latent representation is compatible with the object detection model from [5], which could ultimately enable semantic 3D reconstruction.

Acknowledgments. This work was funded by the Deutsche Forschungsgemeinschaft (DFG, German Research Foundation) in the SFB Transregio 161 ‘Quantitative Methods for Visual Computing’ (Project-ID 251654672) and the Cluster of Excellence ‘Centre for the Advanced Study of Collective Behaviour’.

References

- [1] Federica Bogo, Javier Romero, Matthew Loper, and Michael J. Black. FAUST: Dataset and evaluation for 3D mesh registration. In *Proceedings IEEE Conf. on Computer Vision and Pattern Recognition (CVPR)*, Piscataway, NJ, USA, June 2014. IEEE. 1, 6, 7
- [2] Andrew Brock, Theodore Lim, J. M. Ritchie, and Nick Weston. Generative and discriminative voxel modeling with convolutional neural networks, 2016. 2
- [3] Michael M. Bronstein, Joan Bruna, Taco Cohen, and Petar Veličković. Geometric deep learning: Grids, groups, graphs, geodesics, and gauges. <https://arxiv.org/abs/2104.13478>, 2021. 2
- [4] Joan Bruna, Wojciech Zaremba, Arthur Szlam, and Yann Lecun. Spectral networks and locally connected networks on graphs. In *International Conference on Learning Representations (ICLR2014), CBLIS, April 2014*, 2014. 2
- [5] Nicolas Carion, Francisco Massa, Gabriel Synnaeve, Nicolas Usunier, Alexander Kirillov, and Sergey Zagoruyko. End-to-end object detection with transformers. In Andrea Vedaldi, Horst Bischof, Thomas Brox, and Jan-Michael Frahm, editors, *Computer Vision – ECCV 2020*, pages 213–229, Cham, 2020. Springer International Publishing. 2, 8
- [6] Rohan Chabra, J. E. Lenssen, Eddy Ilg, Tanner Schmidt, J. Straub, S. Lovegrove, and Richard A. Newcombe. Deep local shapes: Learning local sdf priors for detailed 3d reconstruction. In *ECCV, 2020*. 1, 3
- [7] Angel X. Chang, Thomas Funkhouser, Leonidas Guibas, Pat Hanrahan, Qixing Huang, Zimo Li, Silvio Savarese, Manolis Savva, Shuran Song, Hao Su, Jianxiong Xiao, Li Yi, and Fisher Yu. ShapeNet: An Information-Rich 3D Model Repository. Technical Report arXiv:1512.03012 [cs.GR], Stanford University — Princeton University — Toyota Technological Institute at Chicago, 2015. 1, 6
- [8] Zhiqin Chen and Hao Zhang. Learning implicit fields for generative shape modeling. In *Proceedings of the IEEE/CVF Conference on Computer Vision and Pattern Recognition (CVPR)*, June 2019. 1, 3
- [9] Julian Chibane, Thiemo Alldieck, and Gerard Pons-Moll. Implicit functions in feature space for 3d shape reconstruction and completion. In *IEEE Conference on Computer Vision and Pattern Recognition (CVPR)*. IEEE, jun 2020. 1, 2, 3, 5, 6, 8
- [10] Julian Chibane, Aymen Mir, and Gerard Pons-Moll. Neural unsigned distance fields for implicit function learning. In *Advances in Neural Information Processing Systems (NeurIPS)*, December 2020. 3
- [11] Christopher B Choy, Danfei Xu, JunYoung Gwak, Kevin Chen, and Silvio Savarese. 3d-r2n2: A unified approach for single and multi-view 3d object reconstruction. In *Proceedings of the European Conference on Computer Vision (ECCV)*, 2016. 6
- [12] Michaël Defferrard, Xavier Bresson, and Pierre Vandergheynst. Convolutional neural networks on graphs with fast localized spectral filtering. In D. Lee, M. Sugiyama, U. Luxburg, I. Guyon, and R. Garnett, editors, *Advances in Neural Information Processing Systems*, volume 29. Curran Associates, Inc., 2016. 2
- [13] Alexey Dosovitskiy, Lucas Beyer, Alexander Kolesnikov, Dirk Weissenborn, Xiaohua Zhai, Thomas Unterthiner, Mostafa Dehghani, Matthias Minderer, Georg Heigold, Sylvain Gelly, Jakob Uszkoreit, and Neil Houlsby. An image is worth 16x16 words: Transformers for image recognition at scale. In *International Conference on Learning Representations*, 2021. 2
- [14] Nico Engel, Vasileios Belagiannis, and Klaus Dietmayer. Point transformer, 2020. 2
- [15] Fabian B. Fuchs, Daniel E. Worrall, Volker Fischer, and Max Welling. Se(3)-transformers: 3d roto-translation equivariant attention networks. In *Advances in Neural Information Processing Systems 34 (NeurIPS)*, 2020. 2
- [16] Kyle Genova, Forrester Cole, Avneesh Sud, Aaron Sarna, and Thomas Funkhouser. Local deep implicit functions for 3d shape. In *Proceedings of the IEEE/CVF Conference on Computer Vision and Pattern Recognition*, pages 4857–4866, 2020. 3, 8
- [17] Justin Gilmer, Samuel S. Schoenholz, Patrick F. Riley, Oriol Vinyals, and George E. Dahl. Neural message passing for quantum chemistry. In *Proceedings of the 34th International Conference on Machine Learning - Volume 70, ICML'17*, page 1263–1272. JMLR.org, 2017. 2
- [18] Shunwang Gong, Lei Chen, Michael Bronstein, and Stefanos Zafeiriou. Spiralnet++: A fast and highly efficient mesh convolution operator, 2019. 2
- [19] Benjamin Graham, Martin Engelcke, and Laurens van der Maaten. 3d semantic segmentation with submanifold sparse convolutional networks, 2017. 2
- [20] Amos Gropp, Lior Yariv, Niv Haim, Matan Atzmon, and Yaron Lipman. Implicit geometric regularization for learning shapes. In *Proceedings of Machine Learning and Systems 2020*, pages 3569–3579. 2020. 3
- [21] Meng-Hao Guo, Jun-Xiong Cai, Zheng-Ning Liu, Tai-Jiang Mu, Ralph R. Martin, and Shi-Min Hu. Pct: Point cloud transformer, 2021. 2, 4
- [22] Yulan Guo, Hanyun Wang, Qingyong Hu, Hao Liu, Li Liu, and Mohammed Bennamoun. Deep learning for 3d point clouds: A survey, 2020. 2
- [23] Pim De Haan, Maurice Weiler, Taco Cohen, and Max Welling. Gauge equivariant mesh cnns: Anisotropic convolutions on geometric graphs. In *International Conference on Learning Representations*, 2021. 2
- [24] Michael Hutchinson, Charline Le Lan, Sheheryar Zaidi, Emilien Dupont, Yee Whye Teh, and Hyunjik Kim. Lietransformer: Equivariant self-attention for lie groups. <https://arxiv.org/abs/2012.10885>, 2020. 2
- [25] Christian Häne, Shubham Tulsiani, and Jitendra Malik. Hierarchical surface prediction for 3d object reconstruction. In *2017 International Conference on 3D Vision (3DV)*, pages 412–420, 2017. 2
- [26] Sergey Ioffe and Christian Szegedy. Batch normalization: Accelerating deep network training by reducing internal covariate shift. In Francis Bach and David Blei, editors, *Proceedings of the 32nd International Conference on Machine*

- Learning*, volume 37 of *Proceedings of Machine Learning Research*, pages 448–456, Lille, France, 07–09 Jul 2015. PMLR. 4, 5
- [27] Chiyu “Max” Jiang, Avneesh Sud, Ameesh Makadia, Jingwei Huang, Matthias Niessner, and Thomas Funkhouser. Local implicit grid representations for 3d scenes. In *Proceedings of the IEEE/CVF Conference on Computer Vision and Pattern Recognition (CVPR)*, June 2020. 1, 3
- [28] Diederik P. Kingma and Jimmy Ba. Adam: A method for stochastic optimization. In Yoshua Bengio and Yann LeCun, editors, *3rd International Conference on Learning Representations, ICLR 2015, San Diego, CA, USA, May 7-9, 2015, Conference Track Proceedings*, 2015. 6
- [29] Thomas N. Kipf and Max Welling. Semi-supervised classification with graph convolutional networks. In *International Conference on Learning Representations (ICLR)*, 2017. 2
- [30] Renjie Liao, Yujia Li, Yang Song, Shenlong Wang, Charlie Nash, William L. Hamilton, David Duvenaud, Raquel Urtasun, and Richard Zemel. Efficient graph generation with graph recurrent attention networks. In *NeurIPS*, 2019. 2
- [31] Lingjie Liu, Jiatao Gu, Kyaw Zaw Lin, Tat-Seng Chua, and Christian Theobalt. Neural sparse voxel fields. *NeurIPS*, 2020. 8
- [32] William E. Lorensen and Harvey E. Cline. Marching cubes: A high resolution 3d surface construction algorithm. In *Proceedings of the 14th Annual Conference on Computer Graphics and Interactive Techniques, SIGGRAPH ’87*, page 163–169, New York, NY, USA, 1987. Association for Computing Machinery. 6
- [33] Jonathan Masci, D. Boscaini, M. Bronstein, and P. Vndergheynst. Geodesic convolutional neural networks on riemannian manifolds. *2015 IEEE International Conference on Computer Vision Workshop (ICCVW)*, pages 832–840, 2015. 2
- [34] Lars Mescheder, Michael Oechsle, Michael Niemeyer, Sebastian Nowozin, and Andreas Geiger. Occupancy networks: Learning 3d reconstruction in function space. In *Proceedings IEEE Conf. on Computer Vision and Pattern Recognition (CVPR)*, 2019. 1, 2, 3, 6
- [35] Ben Mildenhall, Pratul P. Srinivasan, Matthew Tancik, Jonathan T. Barron, Ravi Ramamoorthi, and Ren Ng. Nerf: Representing scenes as neural radiance fields for view synthesis. In *ECCV*, 2020. 8
- [36] Federico Monti, D. Boscaini, Jonathan Masci, E. Rodolà, Jan Svoboda, and M. Bronstein. Geometric deep learning on graphs and manifolds using mixture model cnns. *2017 IEEE Conference on Computer Vision and Pattern Recognition (CVPR)*, pages 5425–5434, 2017. 2
- [37] Charlie Nash, Yaroslav Ganin, S. M. Ali Eslami, and Peter W. Battaglia. Polygen: An autoregressive generative model of 3d meshes, 2020. 2
- [38] Michael Niemeyer, Lars Mescheder, Michael Oechsle, and Andreas Geiger. Differentiable volumetric rendering: Learning implicit 3d representations without 3d supervision. In *Proceedings IEEE Conf. on Computer Vision and Pattern Recognition (CVPR)*, 2020. 5
- [39] Jeong Joon Park, Peter Florence, Julian Straub, Richard Newcombe, and Steven Lovegrove. DeepSDF: Learning continuous signed distance functions for shape representation, 2019. 1, 3
- [40] Adam Paszke, Sam Gross, Francisco Massa, Adam Lerer, James Bradbury, Gregory Chanan, Trevor Killeen, Zeming Lin, Natalia Gimelshein, Luca Antiga, Alban Desmaison, Andreas Kopf, Edward Yang, Zachary DeVito, Martin Raison, Alykhan Tejani, Sasank Chilamkurthy, Benoit Steiner, Lu Fang, Junjie Bai, and Soumith Chintala. Pytorch: An imperative style, high-performance deep learning library. In H. Wallach, H. Larochelle, A. Beygelzimer, F. d’Alché Buc, E. Fox, and R. Garnett, editors, *Advances in Neural Information Processing Systems*, volume 32. Curran Associates, Inc., 2019. 6
- [41] Songyou Peng, Michael Niemeyer, Lars Mescheder, Marc Pollefeys, and Andreas Geiger. Convolutional occupancy networks. In *European Conference on Computer Vision (ECCV)*, Cham, Aug. 2020. Springer International Publishing. 1, 2, 3, 5, 6, 8
- [42] Charles Ruizhongtai Qi, Hao Su, Kaichun Mo, and Leonidas J. Guibas. Pointnet: Deep learning on point sets for 3d classification and segmentation. *CoRR*, abs/1612.00593, 2016. 2
- [43] Charles Ruizhongtai Qi, Li Yi, Hao Su, and Leonidas J. Guibas. Pointnet++: Deep hierarchical feature learning on point sets in a metric space. *CoRR*, abs/1706.02413, 2017. 2, 4, 8
- [44] Anurag Ranjan, Timo Bolkart, Soubhik Sanyal, and Michael J. Black. Generating 3d faces using convolutional mesh autoencoders. *CoRR*, abs/1807.10267, 2018. 2
- [45] Alexander Rives, Joshua Meier, Tom Sercu, Siddharth Goyal, Zeming Lin, Demi Guo, Myle Ott, C. Lawrence Zitnick, Jerry Ma, and Rob Fergus. Biological structure and function emerge from scaling unsupervised learning to 250 million protein sequences. *bioRxiv*, 2020. 2
- [46] Victor Garcia Satorras, Emiel Hoogeboom, and Max Welling. E(n) equivariant graph neural networks. *CoRR*, abs/2102.09844, 2021. 2
- [47] Shaoshuai Shi, Chaoxu Guo, Li Jiang, Zhe Wang, Jianping Shi, Xiaogang Wang, and Hongsheng Li. Pv-rcnn: Point-voxel feature set abstraction for 3d object detection. In *Proceedings of the IEEE/CVF Conference on Computer Vision and Pattern Recognition (CVPR)*, June 2020. 2
- [48] Vincent Sitzmann, Eric R. Chan, Richard Tucker, Noah Snavely, and Gordon Wetzstein. MetaSDF: Meta-learning signed distance functions. In *arXiv*, 2020. 3
- [49] Vincent Sitzmann, Michael Zollhofer, and Gordon Wetzstein. Scene representation networks: Continuous 3d-structure-aware neural scene representations. In *Advances in Neural Information Processing Systems*, volume 32. Curran Associates, Inc., 2019. 8
- [50] Maxim Tatarchenko, Alexey Dosovitskiy, and Thomas Brox. Octree generating networks: Efficient convolutional architectures for high-resolution 3d outputs, 2017. 2
- [51] M. Tatarchenko, S. R. Richter, R. Ranftl, Z. Li, V. Koltun, and T. Brox. What do single-view 3d reconstruction net-

- works learn? In *IEEE International Conference on Computer Vision and Pattern Recognition (CVPR)*, 2019. 6
- [52] Hugues Thomas, Charles R. Qi, Jean-Emmanuel Deschaud, Beatriz Marcotegui, François Goulette, and Leonidas J. Guibas. Kpconv: Flexible and deformable convolution for point clouds, 2019. 2
- [53] Edgar Tretschk, Ayush Tewari, Vladislav Golyanik, Michael Zollhöfer, Carsten Stoll, and Christian Theobalt. Patchnets: Patch-based generalizable deep implicit 3d shape representations. In Andrea Vedaldi, Horst Bischof, Thomas Brox, and Jan-Michael Frahm, editors, *Computer Vision – ECCV 2020*, pages 293–309, Cham, 2020. Springer International Publishing. 1, 3
- [54] Ashish Vaswani, Noam Shazeer, Niki Parmar, Jakob Uszkoreit, Llion Jones, Aidan N. Gomez, Lukasz Kaiser, and Illia Polosukhin. Attention is all you need, 2017. 2, 5
- [55] Ashish Vaswani, Noam Shazeer, Niki Parmar, Jakob Uszkoreit, Llion Jones, Aidan N Gomez, Łukasz Kaiser, and Illia Polosukhin. Attention is all you need. In I. Guyon, U. V. Luxburg, S. Bengio, H. Wallach, R. Fergus, S. Vishwanathan, and R. Garnett, editors, *Advances in Neural Information Processing Systems*, volume 30. Curran Associates, Inc., 2017. 4
- [56] Shenlong Wang, Simon Suo, Wei-Chiu Ma, Andrei Pokrovsky, and Raquel Urtasun. Deep parametric continuous convolutional neural networks. In *Proceedings of the IEEE Conference on Computer Vision and Pattern Recognition (CVPR)*, June 2018. 2
- [57] Yue Wang, Yongbin Sun, Ziwei Liu, Sanjay E. Sarma, Michael M. Bronstein, and Justin M. Solomon. Dynamic graph cnn for learning on point clouds, 2019. 2
- [58] Wenxuan Wu, Zhongang Qi, and Li Fuxin. Pointconv: Deep convolutional networks on 3d point clouds. In *Proceedings of the IEEE/CVF Conference on Computer Vision and Pattern Recognition (CVPR)*, June 2019. 2
- [59] Qiangeng Xu, Xudong Sun, Cho-Ying Wu, Panqu Wang, and Ulrich Neumann. Grid-gcn for fast and scalable point cloud learning, 2020. 2
- [60] Hengshuang Zhao, Jiaya Jia, and Vladlen Koltun. Exploring self-attention for image recognition. In *Proceedings of the IEEE/CVF Conference on Computer Vision and Pattern Recognition (CVPR)*, June 2020. 2
- [61] Hengshuang Zhao, Li Jiang, Chi-Wing Fu, and Jiaya Jia. Pointweb: Enhancing local neighborhood features for point cloud processing. In *Proceedings of the IEEE/CVF Conference on Computer Vision and Pattern Recognition (CVPR)*, June 2019. 2
- [62] Hengshuang Zhao, Li Jiang, Jiaya Jia, Philip Torr, and Vladlen Koltun. Point transformer. <https://arxiv.org/abs/2012.09164>, 2020. 1, 2, 3, 4, 8